X-622-67-337

NASA TM X-55873

REMARKS ON CLOUD MAPPING BY THE METEOROLOGICAL SATELLITES NIMBUS I AND NIMBUS II

G. KUERS

N67-[illegible]
(ACCESSION NUMBER) (THRU)
37 1
(PAGES) (CODE)
TMX-55873 20
(NASA CR OR TMX OR AD NUMBER) (CATEGORY)
FACILITY FORM 602

GPO PRICE $ _____
CFSTI PRICE(S) $ _____
Hard copy (HC) 3.00
Microfiche (MF) .65
ff 653 July 65

JULY 1967

NASA — GODDARD SPACE FLIGHT CENTER —
GREENBELT, MARYLAND

X-622-67-337

REMARKS ON CLOUD MAPPING BY THE METEOROLOGICAL SATELLITES NIMBUS I AND NIMBUS II

G. Kuers*

July 1967

GODDARD SPACE FLIGHT CENTER
Greenbelt, Maryland

*On leave from the Deutsche Versuchsanstalt für Luft und Raumfahrt E.V. in Oberpfaffenhofen, Germany while with Goddard Space Flight Center as a Resident Research Associate of the National Academy of Sciences – National Research Council.

PRECEDING PAGE BLANK NOT FILMED.

REMARKS ON CLOUD MAPPING BY THE METEOROLOGICAL SATELLITES NIMBUS I AND NIMBUS II

G. Kuers

ABSTRACT

Dense cumulus clouds and fog banks have been selected to determine mean values of their reflectances by means of the High Resolution Radiometers (HRIR) of Nimbus I and Nimbus II in the wavelength region between 3.6μ and 4.2μ. While both instruments yielded satisfactory results during nighttime, it became apparent that Nimbus I delivered too high reflectance values during daytime. From that, it was concluded that false shortwave radiation entered the radiometer. The amount of the energy difference was used to determine the most probable cause of malfunctioning which was considered to be an uncoated rim or a crack of the Interference filter.

PRECEDING PAGE BLANK NOT FILMED.

CONTENTS

PRECEDING PAGE BLANK NOT FILMED.

PRECEDING PAGE BLANK NOT FILMED.

REMARKS ON CLOUD MAPPING BY THE METEOROLOGICAL SATELLITES NIMBUS I AND NIMBUS II

1. INTRODUCTION

One of the Nimbus satellite experiments concerns cloud mapping by the High Resolution Infrared Radiometer (HRIR) which has been described several times (See References 1 to 3). Its spectral region, between 3.6μ and 4.2μ, was originally intended to obtain maps of clouds and the earth during the night, making use of the thermal radiation emitted from them. During daytime, observations with limited accuracy are possible, but the intensities have to be interpreted as reflected solar radiation superimposed on emitted thermal radiation.

Despite the uncertainties of the daytime measurements due to the thermal radiation of the clouds a discrepancy between the results of HRIR I and HRIR II became apparent.

It is the intention of this investigation to find out to what degree the daytime results differ, to consider the various possible sources of error and — since we have no access to the orbiting spacecraft — determine the most probable cause of malfunctioning.

2. SOME PROPERTIES OF CLOUDS WHICH HAVE TO BE CONSIDERED FOR CLOUD ALBEDO COMPARISONS

Since the reflection of solar light by clouds is due to scattering by the cloud droplets according to Mie's theory, the scattered radiation can be expected to be highly anisotropic and therefore dependent on the scattering angle, the droplet size distribution, water content and the thickness of the cloud (See References 4 and 8). An important role is played by the thermal emission of the cloud surface which has a considerable influence on albedo measurements in the spectral region of the HRIR. The measurement can be affected also by the cloud size, if it does not completely fill the radiometer's field of view.

Since we have no immediate information about the physical properties of the observed clouds, we are forced to choose those clouds for the comparisons which seem to have nearly identical radiation features. Fairly well suited for this purpose seem to be extended stratocumuli or fog banks. These types of clouds largely fulfill the requirements of large clouds and can be recognized as heavy water clouds. They should be completely opaque and should not exhibit any noticeable structure. This can best be proved if the background is an ocean surface because it shows nearly no structure in its radiation features.

Stratocumuli and fog show fairly high reflectances and are, therefore, also well suited for determining any difference between the reflectance values obtained from Nimbus I and Nimbus II. However, a disadvantage of these cloud types is in their low heights and associated high temperatures, which results in a considerable amount of thermal radiation leaving the cloud surface and affecting the reflection measurements. This causes an uncertainty in calculation of reflectance. Attempts will be made to get additional temperature measurements from nighttime orbits. In any case, some doubts remain over whether the observed cloud retained its temperature and structure between daytime and nighttime measurements. This is especially true for fog that can even disappear within a few hours — not to speak of its changes of structure.

3. INVESTIGATION OF SOME CLOUDS

HRIR data of both satellites have been selected using the orbit facsimile records which give an immediate and sufficient survey of a complete daytime orbit. Advantage was taken of the Advanced Vidicon Camera System (AVCS) which provides additional visible pictures of the clouds to ensure that the area under observation is indeed a cloud and not perhaps a correspondingly emitting and reflecting ground surface.

Sun and observation zenith angles have to be determined in each case, but only those cases will be selected where both are sufficiently small. Then the observation covers backscattering within a small range of scattering angle.

Investigations of selected clouds have been performed using Mercator Grid Print Maps in 1:1 million scale which contain intensity values in terms of effective temperatures. The choice of the scale has some influence on the readings because extreme values would be smoothed by a more coarse scale.

The effective temperature T_{BB} is related to the effective radiance $\bar{N}$, within the spectral region of the radiometer, by

$$\bar{N} = \int_{\lambda_1}^{\lambda_2} \phi_\lambda B_\lambda(T_{BB})\, d\lambda \qquad (1)$$

where $B_\lambda(T_{BB})$ is the radiance of a blackbody of temperature T_{BB} and ϕ_λ the spectral responsivity of the radiometer. During daytime the effective radiance is

$$\bar{N}_D = \int_{\lambda_1}^{\lambda_2} \phi_\lambda \left[(1 - R) B_\lambda(T_{BB}) + R\, H \cos z/\pi\right] d\lambda . \qquad (2)$$

Here R is the reflectance of the surface under observation. Its wavelength dependency, although present for clouds, can be neglected for comparison purposes. Equation (2) contains the simplifying assumption of isotropically reflecting clouds; therefore, their radiance is $RH\cos z/\pi$ where $H \cos z$ is the irradiance of the cloud and z is the zenith angle of the sun. Neglecting anisotropy does not affect the following evaluations since only cases of scattering angles within a sufficiently small range will be considered.

Equation (2) has been used for plotting a set of curves for which $r = R \cos z$. R itself can readily be obtained if the surface temperature of the cloud is taken into account. Since Nimbus II uses an improved interference filter with higher transmission as well as with higher responsivity at shorter wavelengths (See Figure 1), relation (2) was used separately for each radiometer (See Figures 2 and 3). Higher short wavelength responsivity causes increased effective temperatures for a given albedo.

In order to obtain representative values of cloud albedos from grid print maps frequency distributions of the effective cloud temperatures are studied. The effective cloud temperatures associated with the distribution maxima are considered representative. Besides this, shapes of the frequency distributions yield some information about cloud structures, as we shall see.*

Unfortunately, one case excepted, it was not possible to determine the daytime surface temperature of the clouds by nighttime measurements because they were broken up or even vanished during the time between both measurements. There exists in principle the possibility to determine the surface temperature by simultaneous measurements of the Medium Resolution Radiometer (MRIR) in the 10 to 11 micron channel. However, since this applies only to Nimbus II and since we are primarily interested in resolving the discrepancy between both cloud albedo measurements, we may forgo a precise determination of the surface temperature; moreover, we know that its influence is small in comparison to the relatively high reflected intensity of the clouds. Thus, as a first order approximation, we assume an equal cloud height in every case and estimate the temperature of the cloud by applying an equal temperature gradient to the appropriate sea temperature.

The first case chosen of a cloud observed by Nimbus I was over an area about 8° west of the shore of Chile. The enlarged reprint and the visible picture are shown in Figures 4 and 5. From the frequency distribution in Figure 6, an

*The frequency distribution allows us also to determine the degree of uncertainty of temperature measurements due to noise fluctuations if the radiation field is sufficiently uniform.

effective cloud temperature of 317.5°K can be read off. The steep slopes of the distribution confirm that the cloud has indeed highly uniform radiation features.

Another case observed by Nimbus I was likewise chosen from an area in the South Pacific (See Figures 7 and 8). In Figure 9, four frequency distributions are plotted. Three of them refer to three selected narrow strips, north-south oriented, according to the remarks in Figure 9 and intentionally including areas with broken clouds in the north and the south. The fourth curve refers to one of these regions but does not include broken clouds at the edge of the cloud.

A comparison of one of the broken cloud distributions with that related to the smooth cloud part makes it clear that the temperature corresponding to the maximum of the frequency distribution is really representative of the mean value of the effective temperature because its position is obviously not affected by broken parts of the cloud. These seem only to decrease the steepness of the low temperature slope causing the distribution curve to fall off to the effective temperature of the ocean. We recognize further that the position of the maximum is the same within a longitude range of 9.5° which confirms that the cloud is really highly homogeneous with an effective temperature of 315°K.

Fortunately, it was possible to trace back the cloud system to a nighttime orbit, seven orbits before (Figure 10 shows the reprint and Figure 11 the frequency distribution). From the reprint, three intensity ranges can be clearly discerned. In the south a low emitting region is present, apparently high clouds. The central part of the reprint is grey shadowed showing our cloud system in a southwestern direction of the point where it appeared about twelve hours later. The grey tone and the fairly high homogeneity of the cloudy area confirm that the cloud is one of the low altitude, high emitting type. Only some portions in the north show still higher temperature. Most likely they are spots of open sea unobscured by broken clouds. The mean temperature of the cloud can be read off from the frequency distribution as 278°K.

A third cloud system was selected from the same orbit, not very far south from that discussed at last (See Figures 12 and 8). The frequency distribution in Figure 13 shows that apparently the observed cloud part is also smooth, since the maximum which occurs at about 314°K is fairly well pronounced.

A nighttime observation (See Figure 14) * also about twelve hours earlier, produced a cloud surface temperature measurement of about 280°K, obtained

*The size of the smallest of the grey spots approaches the instrument's resolution, thus simulating a rather uniform cloud size distribution which is probably not present in reality.

from the frequency distribution in Figure 15. It is a remarkable feature of the distribution that a sharp cut-off at about 280°K occurs, while in the direction of higher temperatures it falls off more slowly. An explanation is given by the fact that we have broken clouds which partially obscures the ocean, thus causing the slow fall off to high temperatures while the sharp cut-off indicates the lowest occuring temperature which is most probably the surface temperature of the cloud.

The first case chosen from Nimbus II was a fog bank west of Spain (See Figures 16 and 17). The maximum of the frequency distribution in Figure 18 shows an effective cloud temperature of about 306°K. The slopes are fairly steep, however, the curve seems to be broader than the corresponding curves from Nimbus I.*

As a second case, an extended cloud south of the French Riviera was selected (See Figure 19 and 20). From the AVCS picture, it can be recognized that South Europe, the Mediterranian Sea, and North Africa are covered with dense haze. Less pronounced, but still recognizable is the haze layer in the enlarged reprint where it occurs as dark spots, especially over Spain and a large one over the Mediterranian Sea and the coast of Africa. It is, therefore, to be expected that the frequency distribution will not be as smooth as in the foregoing cases. However, as Figure 21 shows, it even possesses three maxima. That they are real has been proved by counting several times slightly different areas. A possible explanation is given by the assumption that the maxima are related to three different reflecting layers, the ocean, the cloud and the haze layer, with the last two being not quite opaque or at least having transparent areas. Since it is not quite clear how the maxima came about, the maximum at 305° K shall be taken for the present as a representative value of the effective temperature.

A third case was selected from the same orbit, west of Spain. A cloud occurs there, separated from the land only by a small strip of open sea. The effective temperature can be read off as 305°K (See Figure 22).

It appears that the other cases of Nimbus II also show somewhat broader distributions. This may be expected, since the effective radiance is always smaller, and, therefore, — with detectors of the same D — the signal to noise ratio is lower than for Nimbus I, and since the width of the curve is related to the signal-to-noise ratio.

4. COMPARISON OF DAYTIME RESULTS OF BOTH RADIOMETERS

Evaluation of cloud reflectances has been performed, assuming an equal cloud height of 2000 meters, a vertical temperature gradient of 6°/km and taking into account the monthly mean value of the ocean's temperature.

Reflectance values obtained from Nimbus I range between 22.8% and 32.4%. The mean value of the reflectance is 26.6% and the appropriate effective radiance is 3.2×10^{-5} Wcm^{-2} sr^{-1}.

Concerning Nimbus II, the cloud reflectance range between 12.5% and 13.6%. The mean value is 12.9% and the effective radiance is 2.7×10^{-5} Wcm^{-2} sr^{-1}. The difference of radiance which has to be discussed now is 5×10^{-6} Wcm^{-2} sr^{-1}.

The discrepancy exists only during daytime. Allison and Kennedy (See Reference 9) have compared nighttime measurements over oceans, performed by Nimbus I, with those carried out from ships and airplanes, and they found satisfactory agreement. Thus it seems that the malfunctioning depends on the presence of the intensive solar short wavelength radiation. That means the wavelength responsivity of one (or both) of the radiometers is different from the assumed one. Since the detector is used at its responsivity peak and since an interference filter with a relatively small bandwidth is employed, a change of the spectral transmittance of the filter is much more probable than a change of the detector's sensitivity.

Another question arises in this connection, namely which of the HRIR's may have delivered erroneous results. Comparisons of the HRIR data with cloud reflectance values obtained by Blau et al., (See Reference 5) seem to indicate that cloud reflectances should not exceed values of the order of 6% (See Figure 23). Accurate conclusions cannot be drawn from Blau's results because his investigations do not go beyond 3.6 μ and moreover because they are in disagreement with his later investigations which yielded higher values. Nevertheless, it shall be assumed that the erroneous values are those of Nimbus I, partly because this allows us to explain the discrepancy in an unconstrained manner.

The following possible sources of error seem worthy of investigation now:

1. Assumption of additional transmission peaks of the filter at short wavelengths.

2. Assumption of a filter shift towards shorter wavelengths.

3. Assumption of additional unfiltered radiation reaching the detector.

4.1 Assumption of Additional Transmission Peaks of the Filters

The filters of both HRIR's have been very carefully measured by the manufacturer (See Reference 6) before they were mounted. Besides this, filters of the same batch have been once more checked after the discrepancy became obvious. In no case was it possible to detect a secondary transmission of more than 0.01%. Thus, it seems highly improbable that the error has been caused by additional transmission peaks.

4.2 Filter Shift Assumption

In order to estimate the influence of a spectral filter shift, the relation between the relative error of reflectance and the wavelength shift has been calculated and plotted in Figure 24, assuming — for an easier calculation — a rectangular shaped filter transmission curve. Since the reflectance value obtained by Nimbus I is more than 100% higher than that obtained by Nimbus II, a shift of more than 0.2μ would be needed for an explanation. As Figure 24 explains further, this filter shift towards shorter wavelengths would at the same time cause nighttime temperatures which are about 10°K too low. Since this has at no time been observed as the investigations of Allison and Kennedy have shown, a filter shift is also highly improbable. Moreover a shift to this extent could hardly be explained. In principle, it could be caused by tilting the filter or by appropriate variations of its temperature. As investigations of Illsley (See Reference 7) explain, the tilting angle and the temperature deviation must be likewise improbably high. Thus an explanation by a wavelength shift is also, from this standpoint, hardly possible, because we know that the variation of the housing temperatures of the radiometers are not higher than a few degrees, and great tilting angles cannot be explained with respect to the layout of the filter mounting.

4.3 Assumption of Additional Unfiltered Radiation

It seems not very likely that the error could be caused by direct sunlight entering the radiometer at the sun oriented side through a defective housing, because the Nimbus spacecraft shields it from direct sun radiation. Moreover, the measured values should depend on the incidence angle of the sunlight which in fact was not the case, but the recorded intensity follows the nadir angle in a quite striking manner.

False light may also have reached the detector by passing through peeled-off parts of the filter. The percentage of the peeled-off filter area that is related to the radiance of 5×10^{-6} Watts cm^{-2} sr^{-1} has been calculated, assuming the following conditions:

Isotropic cloud reflectance between 1.5μ and 2.5μ of about 50% (after Hewson, see Reference 8).

Total atmospheric water content of about 6 mm ppt water.

Short wavelength cut off by the Ge — substrate of the filter at 1.5μ.

The windows between 1.5μ and 1.8μ and between 2.0μ and 2.5μ together contribute, under these assumptions, additional reflected radiation of $1{,}50 \times 10^{-6}$ Watts cm^{-2} sr^{-1}. The percentage of peeled-off filter area necessary is 0.3%. Taking into account the filter size, the value would be equivalent to an uncoated circular spot of 2.5 mm diameter, corresponding to an area of 5 mm^2. It seems highly improbable that a peeling of this amount could have been caused by scratching. It seems more likely that this uncoated area comes from at least a part of the uncoated rim which every interference filter has on account of the manufacturing process. This ring shaped area which generally shows a width of one or two mm ought to be completely covered by the mounting. An estimate shows that a ring with a width of 0.05 mm, uncovered by the filter mounting is sufficient to explain the discrepancy. Since, unfortunately, both instruments have not been tested with short wavelength radiation before launch, this explanation possesses a high probability.

Another question may arise; namely, whether the filter has suffered a crack, for instance during launch. In this case the faulty area can be even smaller due to the fact that now still more sunlight, down to about 0.4μ, at increased cloud reflectance, can reach the detector. Again, taking into account the dimensions of the filter a gap of only 0.03 mm is sufficient, if the filter should have broken in two parts. It frequently occurs that filters which are subject to a shock break into just two parts, where both parts stay in their position and are separated by a very small gap.

5. CONCLUSION

Three cases of observation of high reflecting clouds have been investigated for each HRIR by means of frequency distributions. A mean value of cloud reflectance has been derived for each radiometer and the intensity difference between both has been determined.

On account of the nearly complete lack of reliable published cloud reflectance data in the wavelength region in question, it was assumed that the HRIR of Nimbus I was malfunctioning (resulting in too high effective temperatures) because this leads to a reasonable explanation for the discrepancy between the

two HRIR measurements. It certainly cannot be expected that the error can be located in a straightforward manner, because we have no access to the orbiting spacecraft. But it is possible to give explanations which are more or less likely on account of the excess of intensity recorded by Nimbus I. After all, the most probable explanation seems to be the assumption of an unlaminated filter area at the rim of the filter which every interference filter shows and which in the case of Nimbus I was possibly not completely covered by the filter mounting, thus allowing the short wavelength radiation to pass through the unlaminated filter area. Another assumption explains the excess intensity by a cracked filter causing short wavelength radiation to penetrate the filter through the crack.

We will leave open the question as to whether the filter was improperly mounted or cracked. Both explanations may likewise be possible. However, if it should become evident that Nimbus II has also given too high values, the explanation by the unlaminated area seems more likely — if we don't want to assume that both filters were cracked.

Although it was not possible to make definite decisions, it should at least be obvious that it is advisable to test future HRIR with short wavelength radiation also.

ACKNOWLEDGMENTS

The author wishes to thank Mr. William R. Bandeen for his suggestions and discussions. The interest and the contributions of Dr. Robert Samuelson, Mr. Lonnie Foshee and Mr. Lewis Allison are also very much appreciated.

REFERENCES

1. Catalog and User's Manual of Nimbus I and Nimbus II, NASA, Goddard Space Flight Center, 1965 and 1966.

2. Observations from the Nimbus I Meteorological Satellite, NASA Special Publication No. 89, 1965.

3. Widger, W. K., Jr., Barnes, J. C., Merritt, E. S., Smith, R. B., Meteorological Interpretation of Nimbus High Resolution.

4. McDonald, R. K., Deltenre, R. W., Cirrus Infrared Reflection Measurements. JOSA, v 53, p. 860 (1963).

5. Blau, H. H., Jr., Duchane, E. M., et al. Infrared Spectral Properties of High Altitude Clouds. Contract No. NONR 3556 (00), (1963).

6. Personal Communication with the manufacturer of interference filters.

7. Illsley, R. F., Preliminary Study of Low Temperature Effect on Interference Filters. Presentation at IRIS meeting, April 20, 1960.

8. Hewson, E. W., The Reflection, absorption and Transmission of Solar Radiation by Fog and Cloud. Roy. Met. Soc. Quart. Journ., v 69 (1943).

9. Allison, L. J., Kennedy, J. S., An Evaluation of Sea Surface Temperature as Measured by the Nimbus I High Resolution Infrared Radiometer. NASA Technical Note, No. G-800.

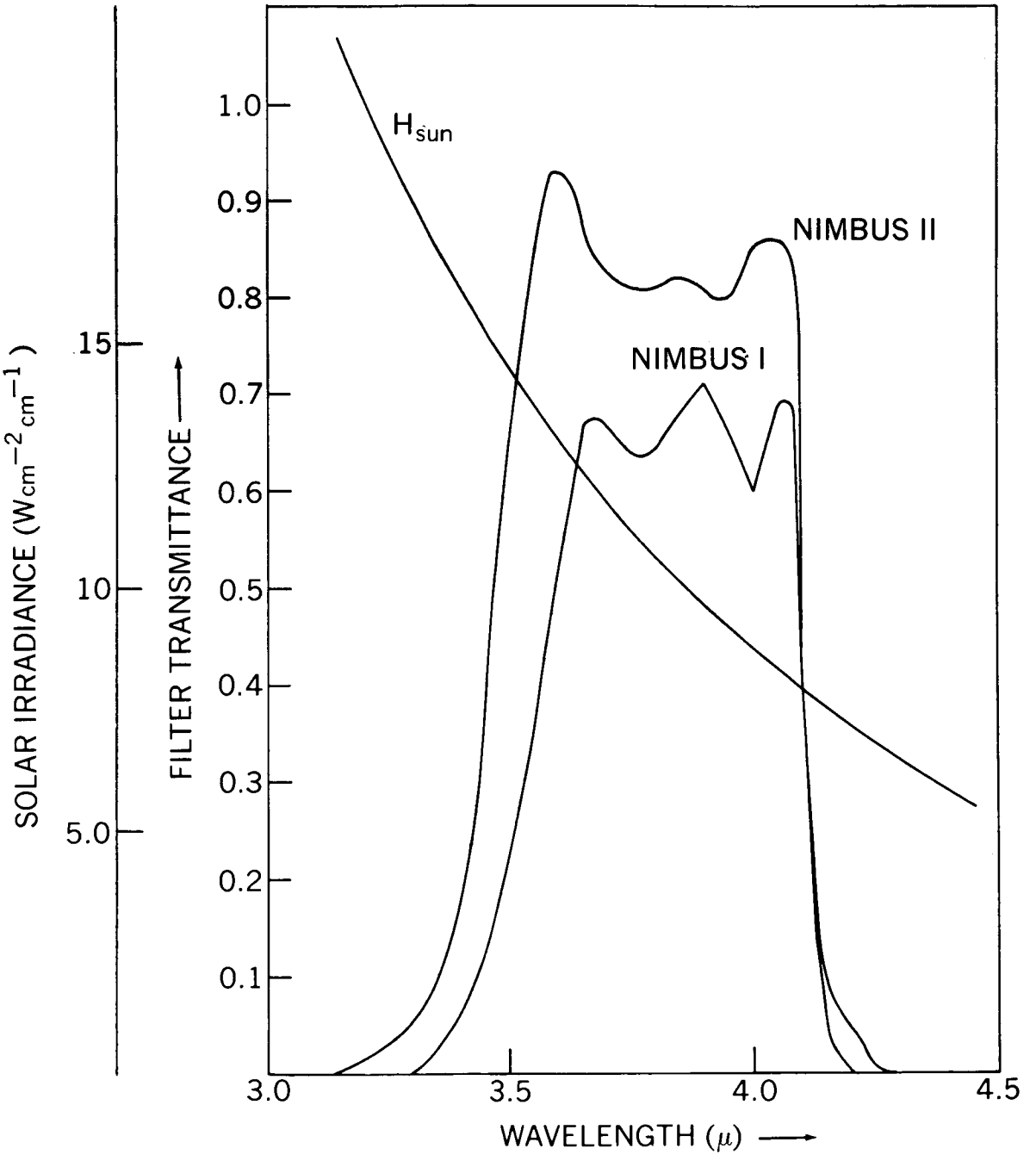

Figure 1. Solar Irradiance and Filter Transmittances of HRIR I and HRIR II

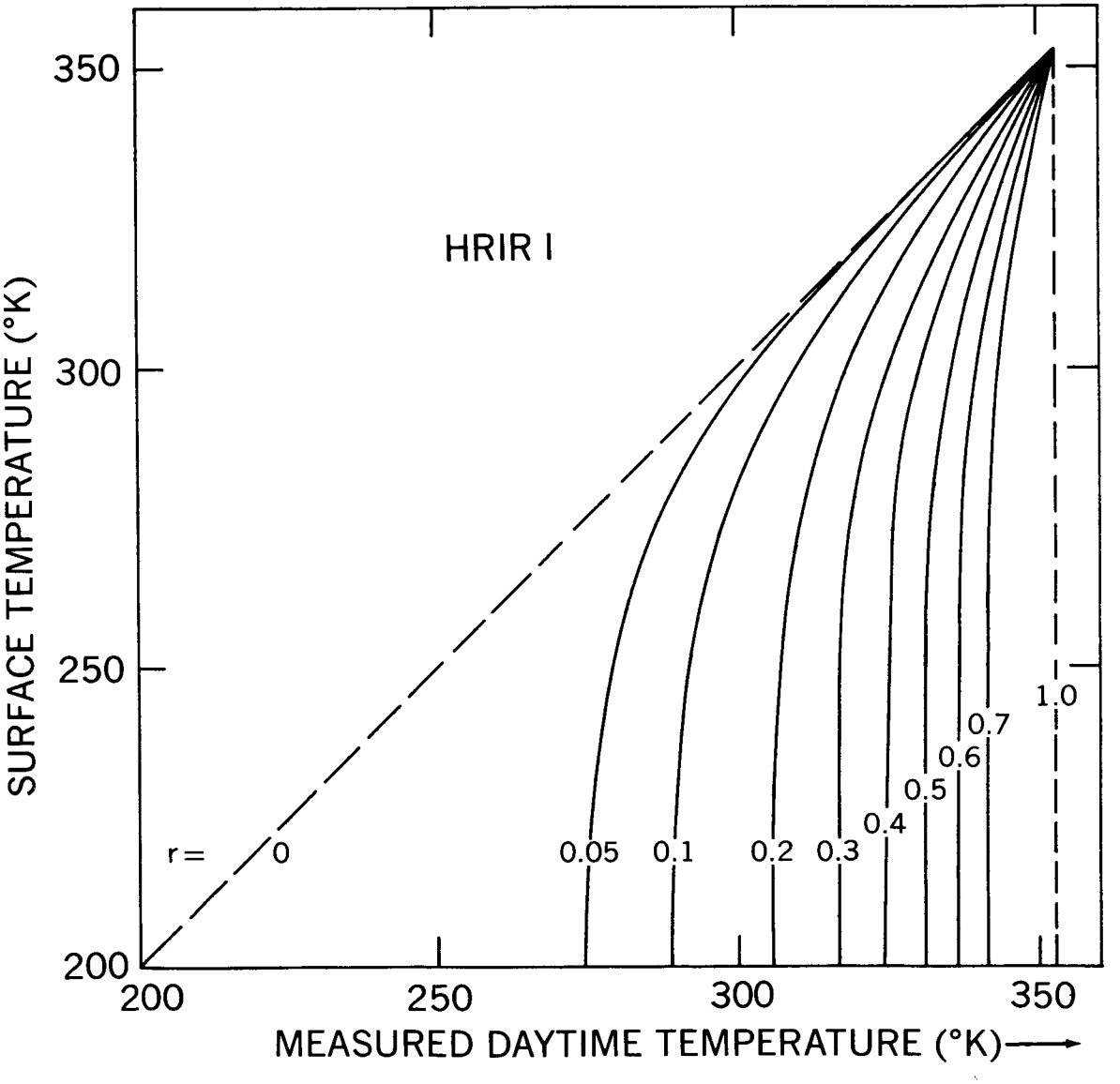

Figure 2. Relation between Reflectance, Surface Temperature and Daytime Temperature, HRIR I

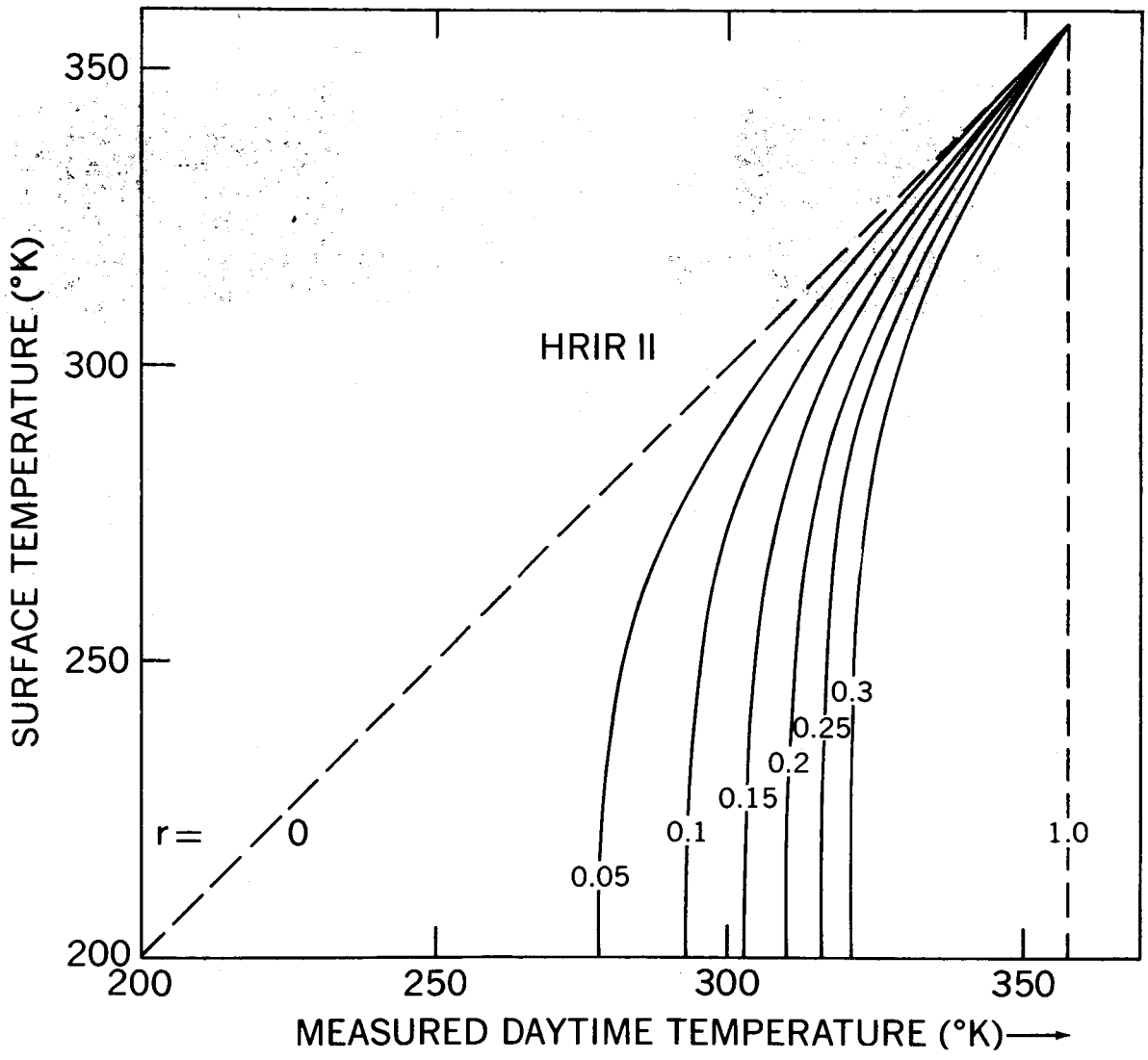

Figure 3. Relation between Reflectance, Surface Temperature and Daytime Temperature, HRIR II

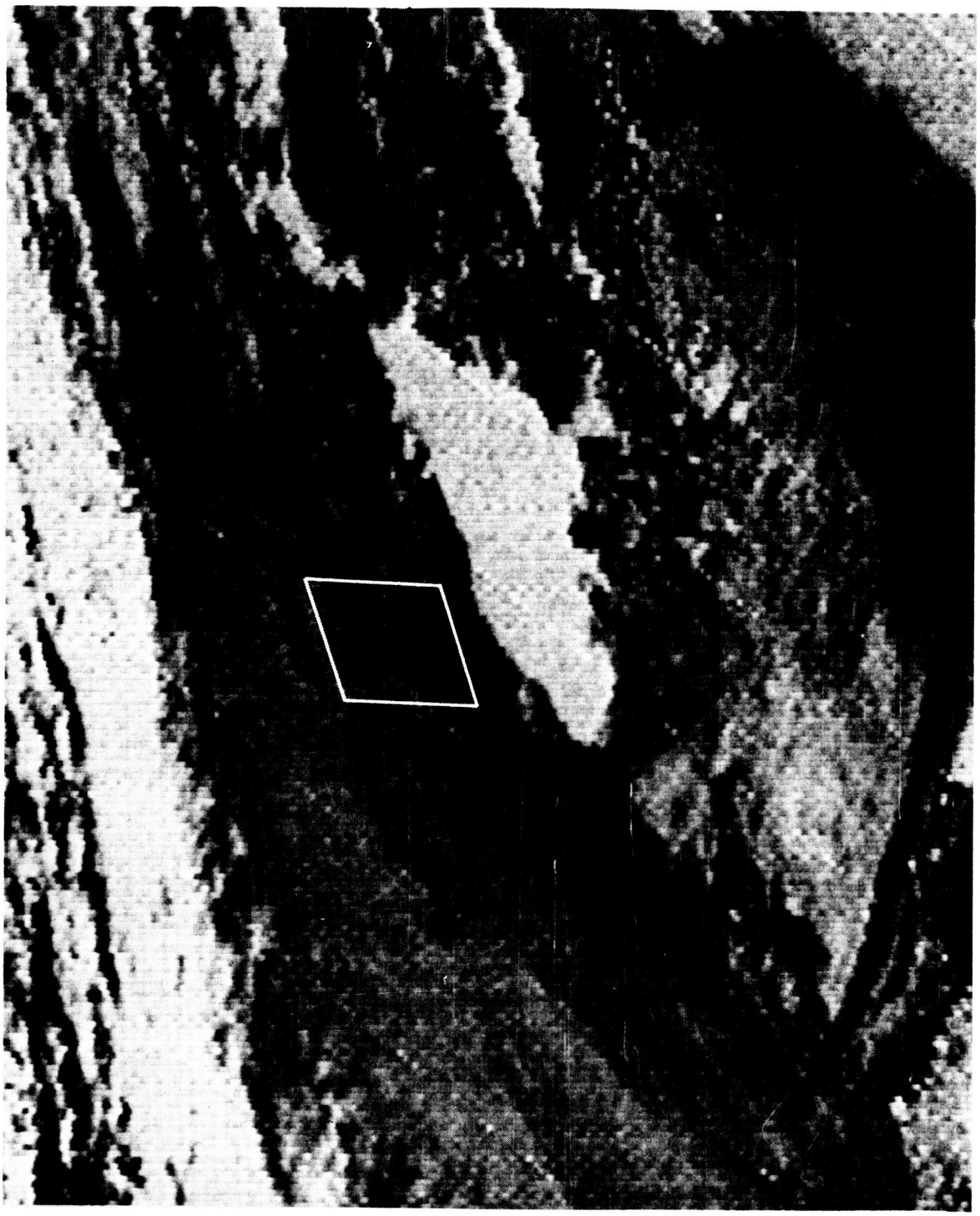

Figure 4. Infrared Photofacsimilie, HRIR I, Sept. 11, 1964, Orbit 210, 36.5° S, 84° W

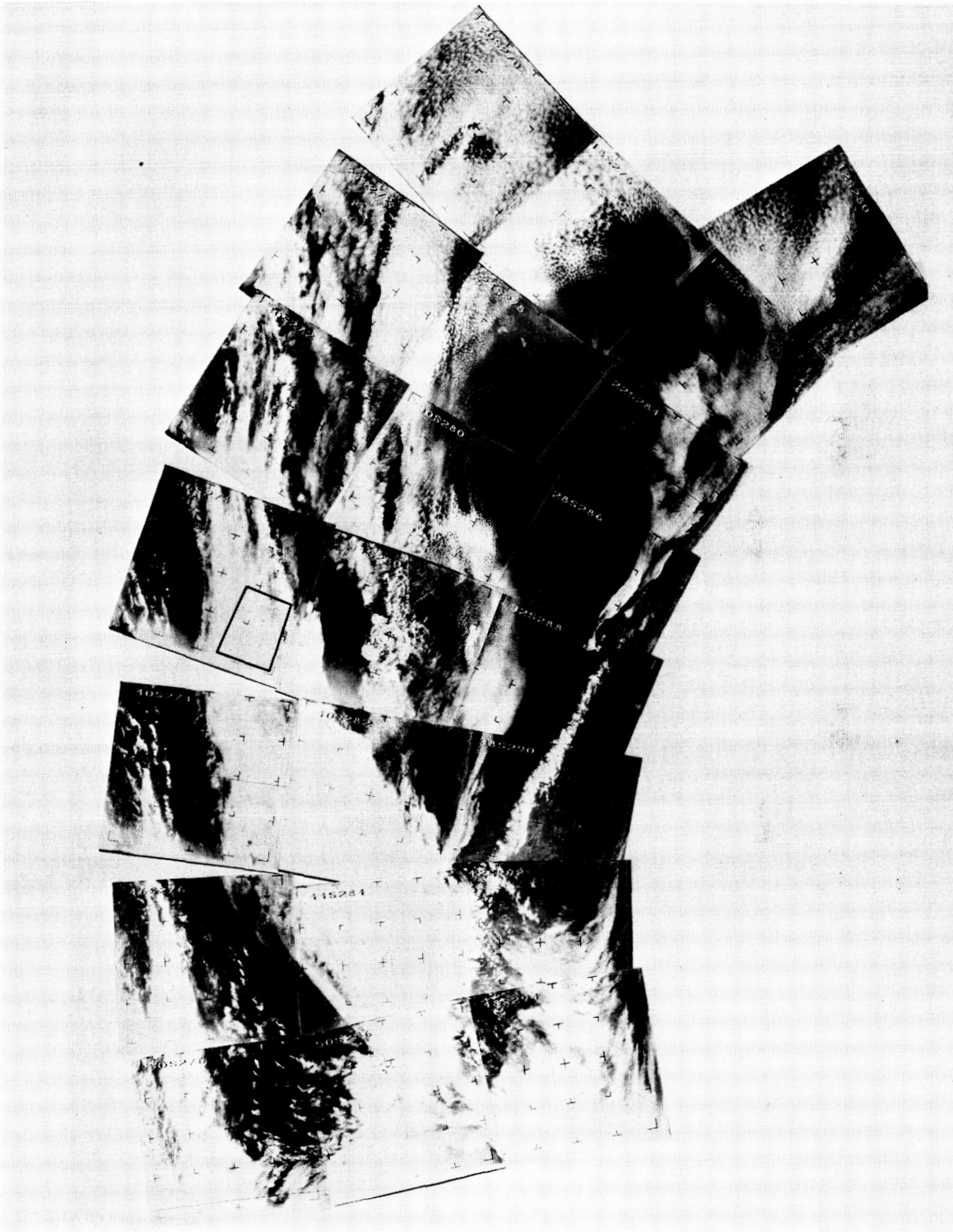

Figure 5. Visible Picture, HRIR I, Sept. 11, 1964, Orbit 210, 36.5° S, 84° W

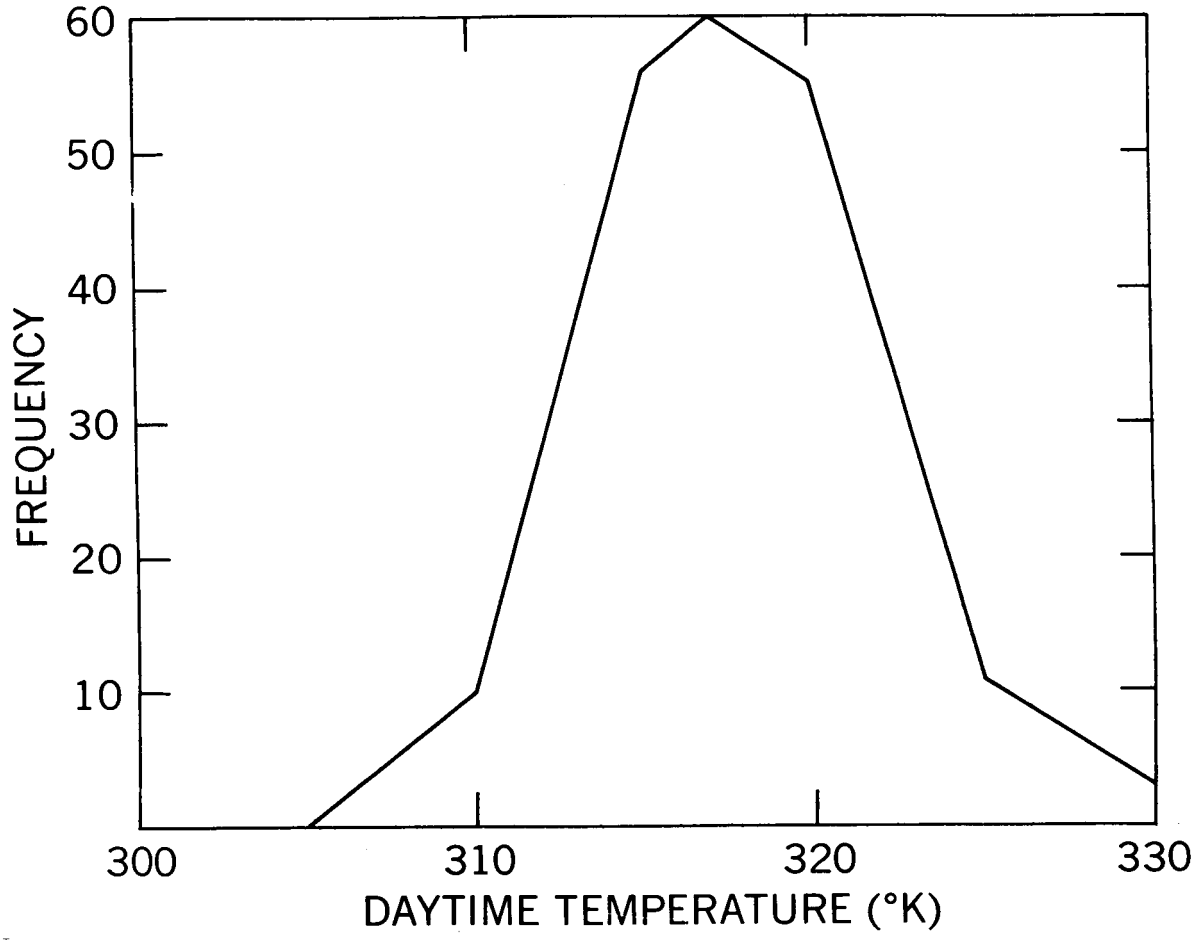

Figure 6. Frequency Distribution of Daytime Temperature, HRIR I, Sept. 11, 1964, Orbit 210, 36.5° S, 84° W

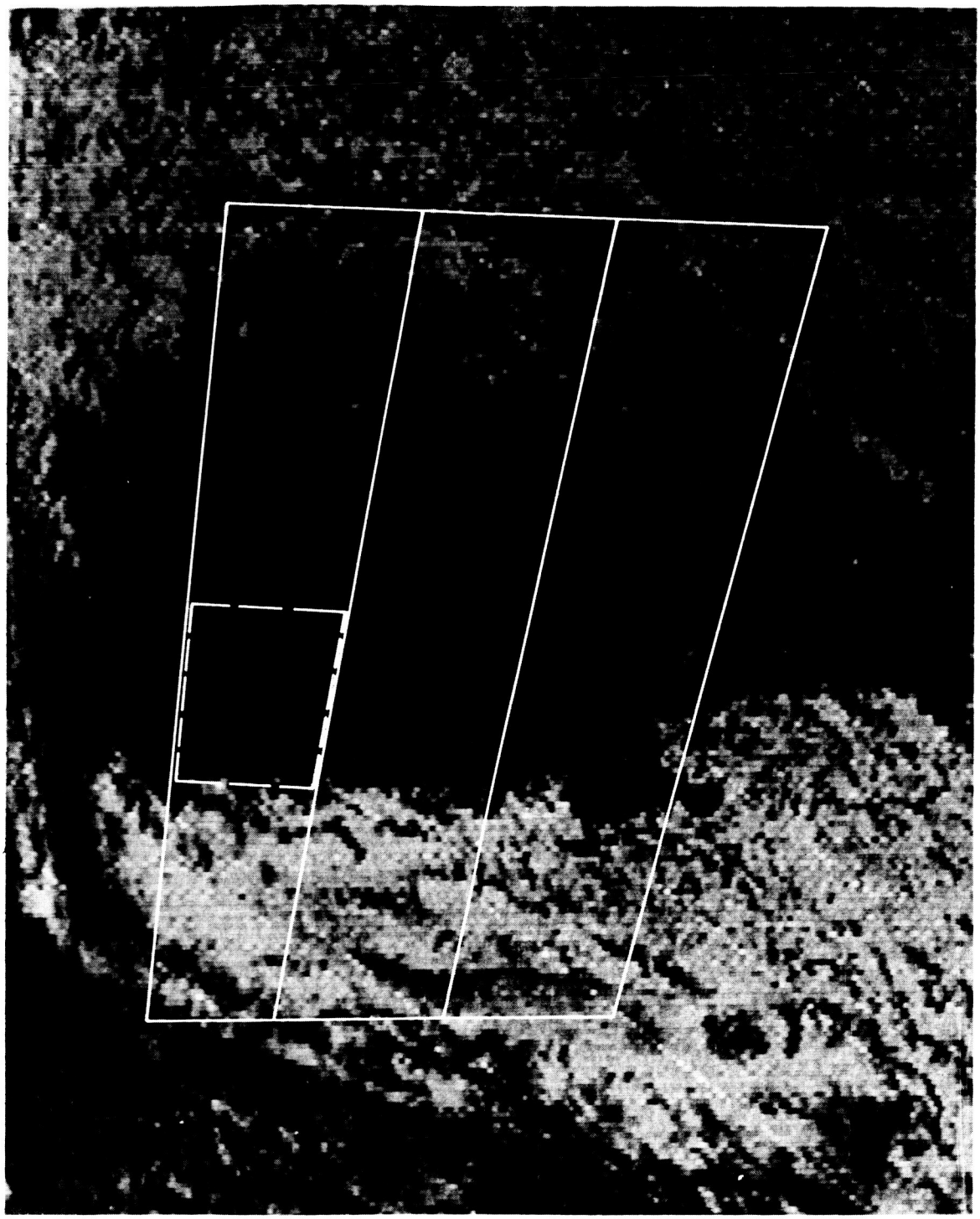

Figure 7. Infrared Photofacsimilie, HRIR I, Sept. 2, 1964, Orbit 80, 27° S, 126° W

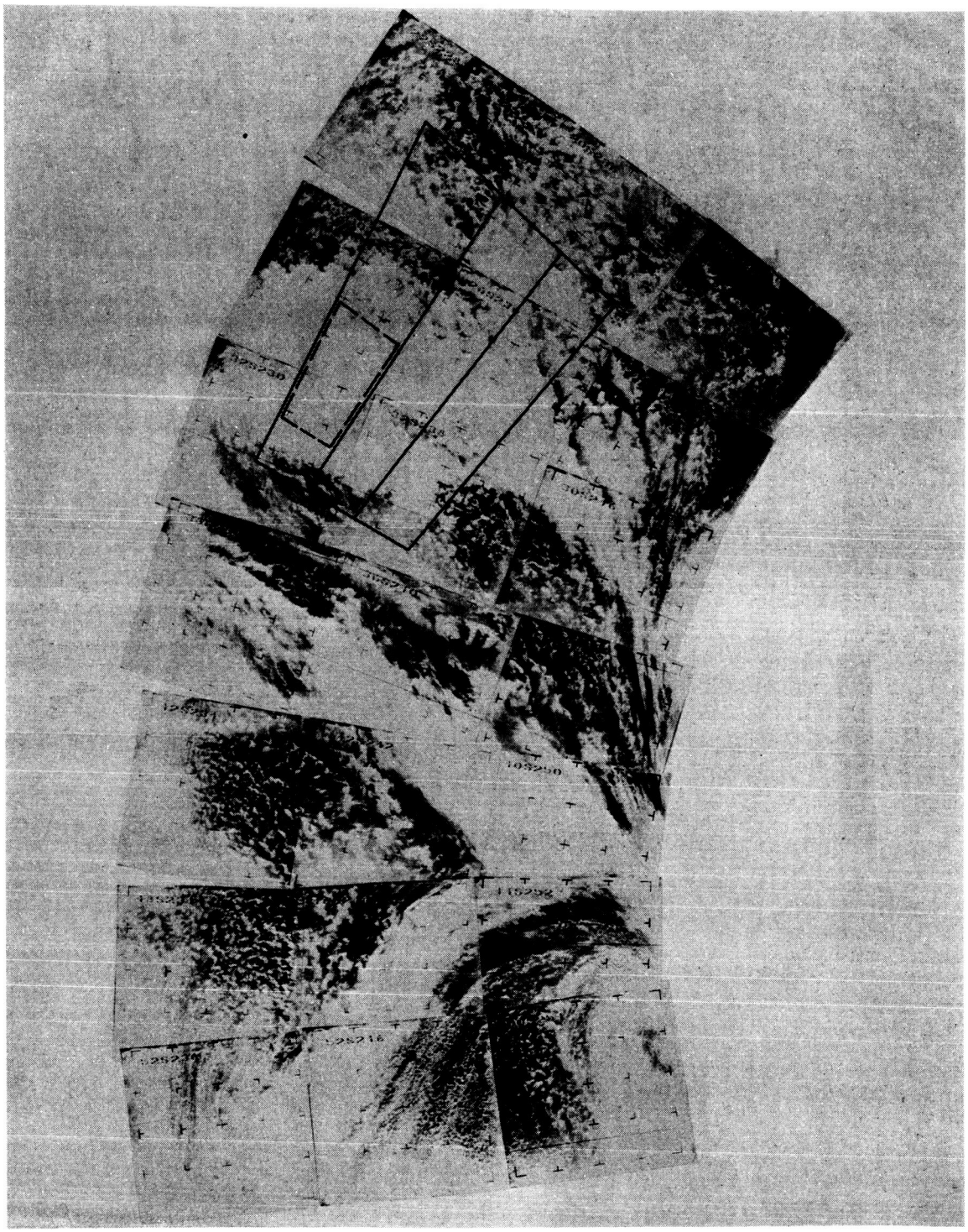

Figure 8. Visible Picture, HRIR I, Sept. 2, 1964, Orbit 80, 27° S, 126° W

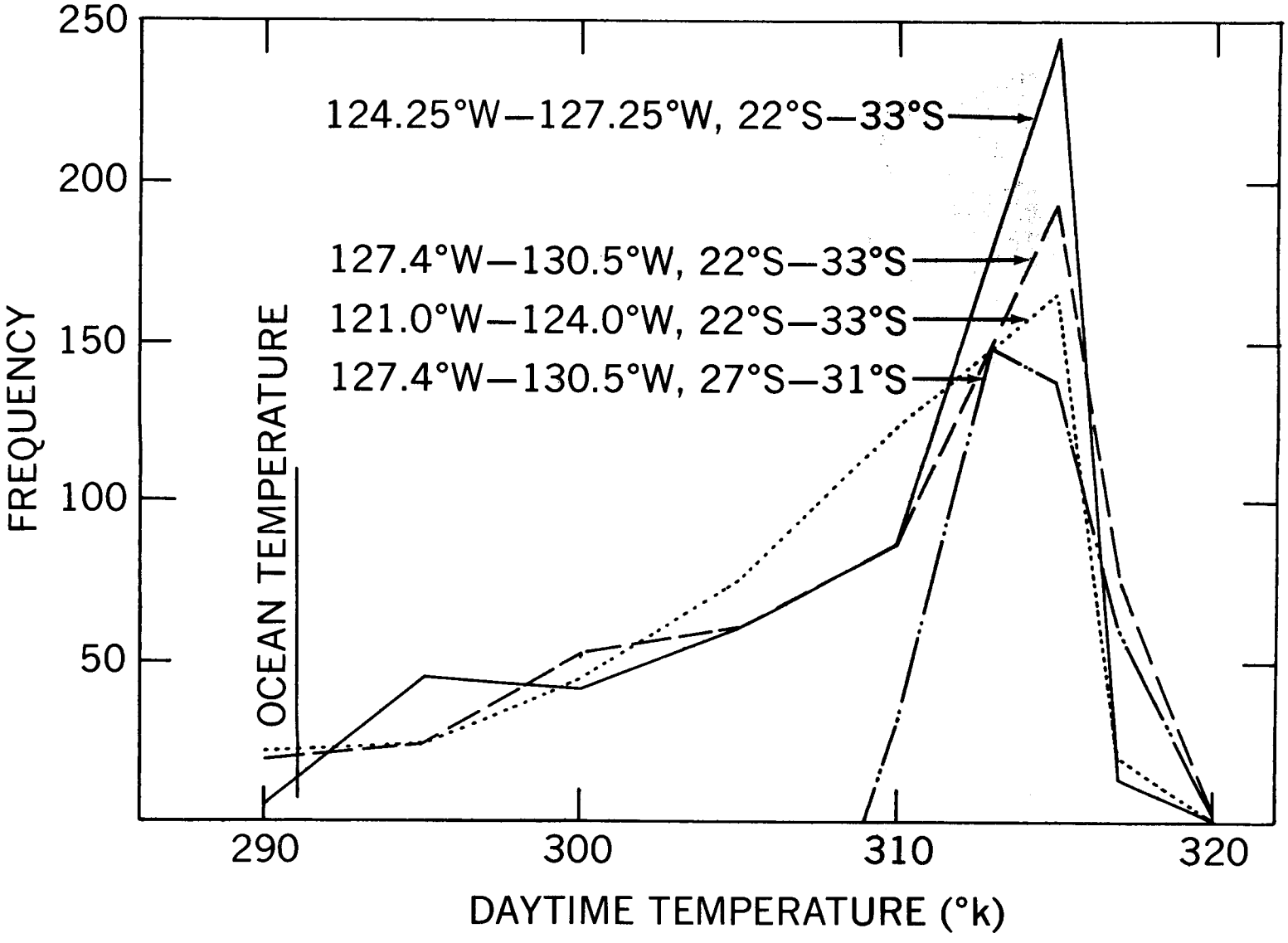

Figure 9. Frequency Distribution of Daytime Temperature, HRIR I, Sept. 2, 1964, Orbit 80, 27° S, 126° W

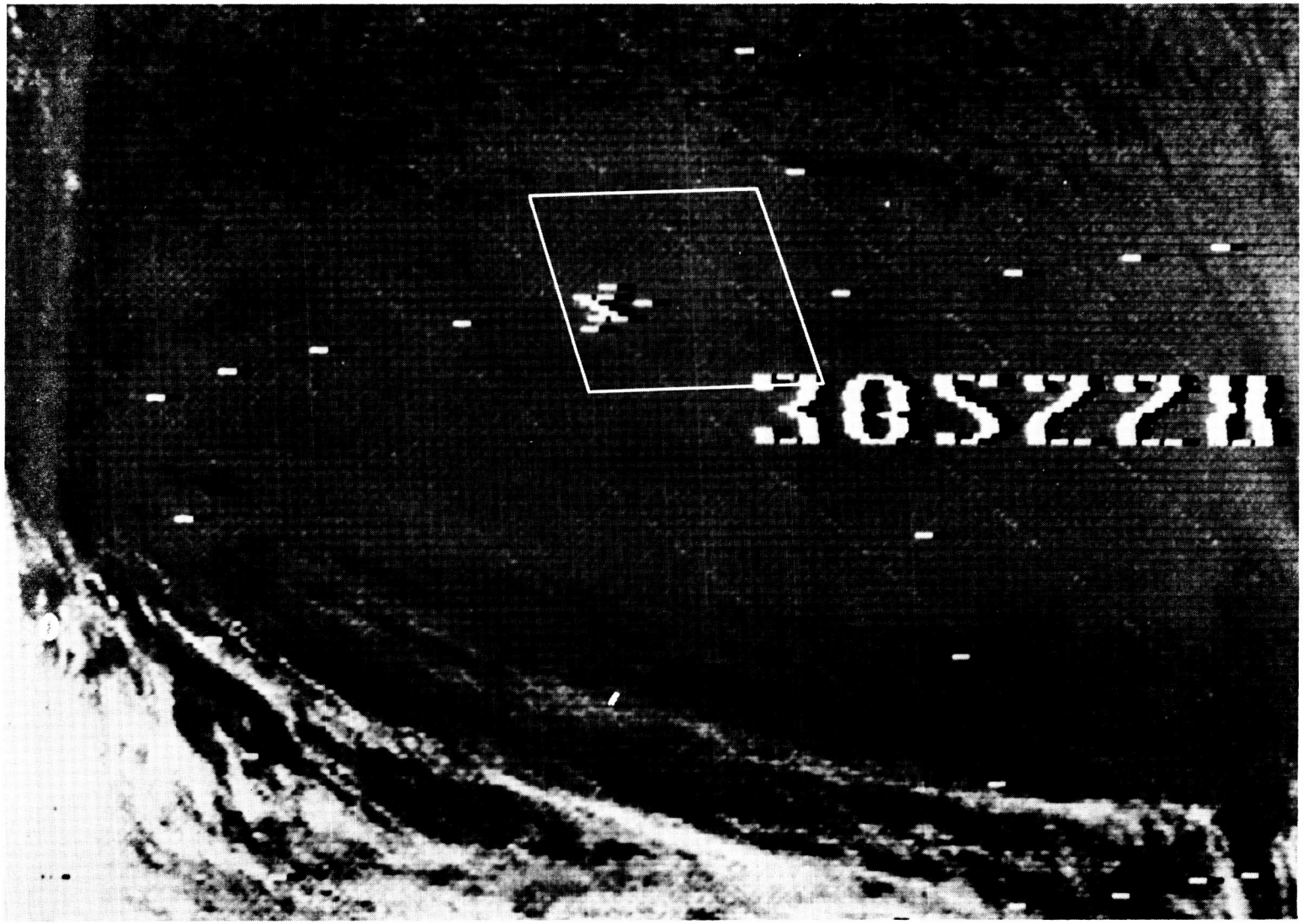

Figure 10. Infrared Photofacsimile, HRIR I, Sept. 2, 1964, Orbit 73, 29.5° S, 132° W

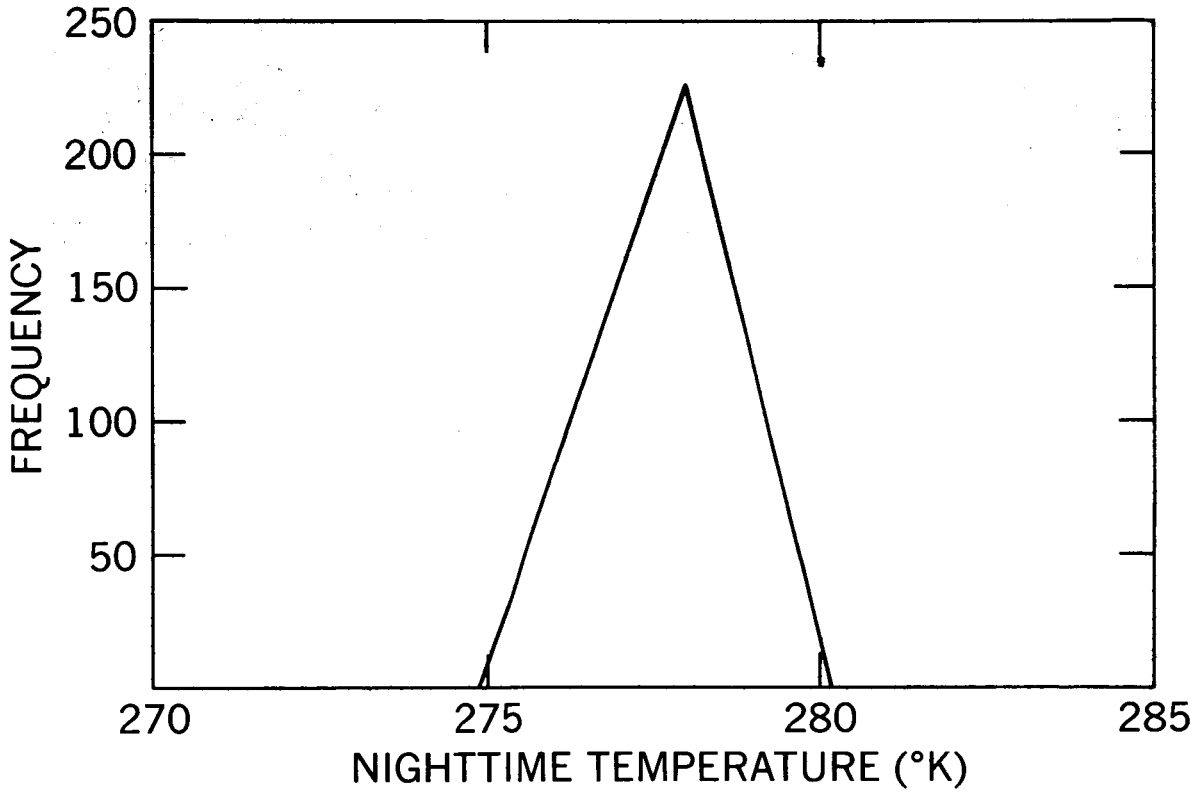

Figure 11. Frequency Distribution of Nighttime Temperature, HRIR I, Sept. 2, 1964, Orbit 73, 29.5° S, 132° W

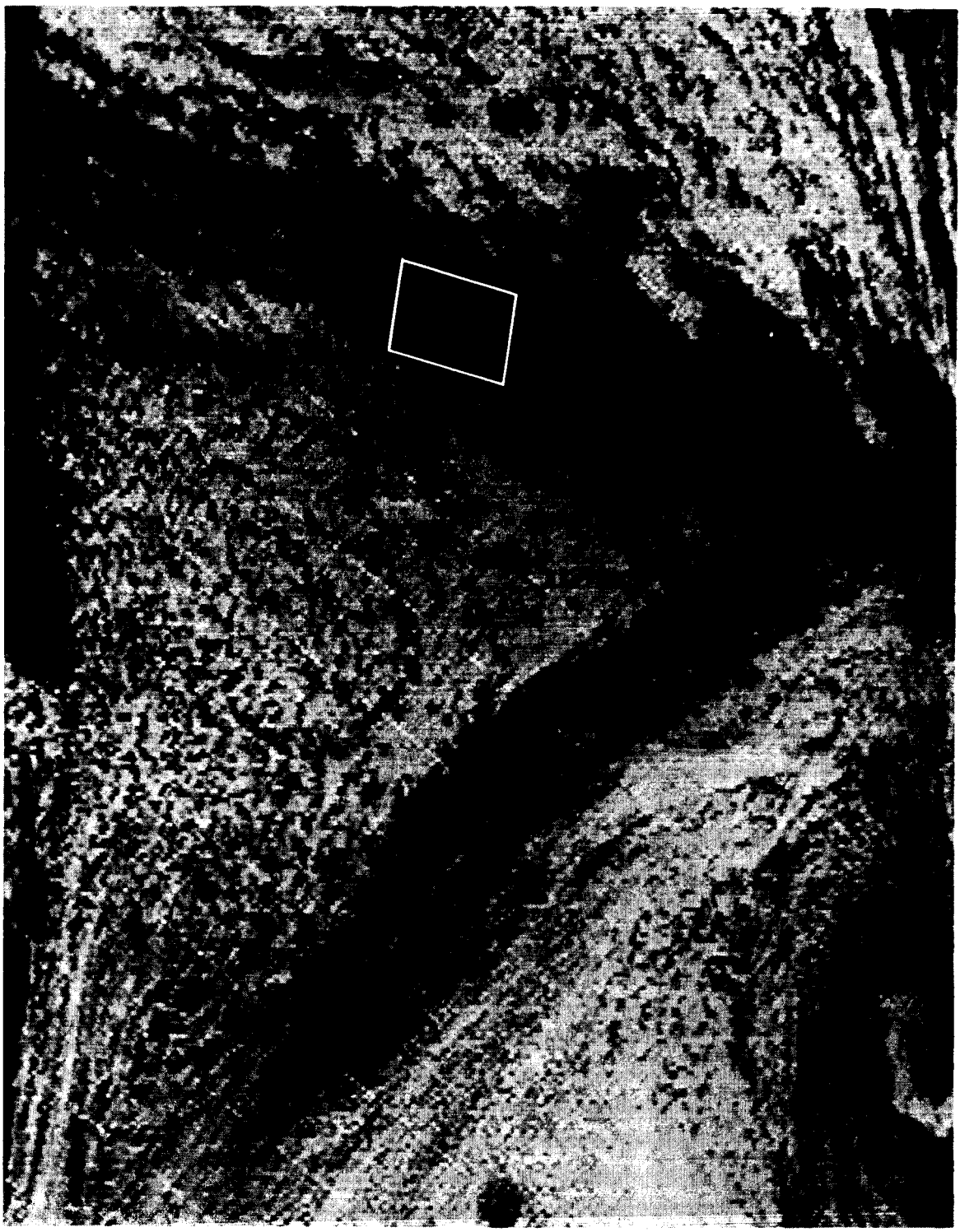

Figure 12. Infrared Photofacsimile, HRIR I, Sept. 2, 1964, Orbit 80, 38° S, 116.5° W

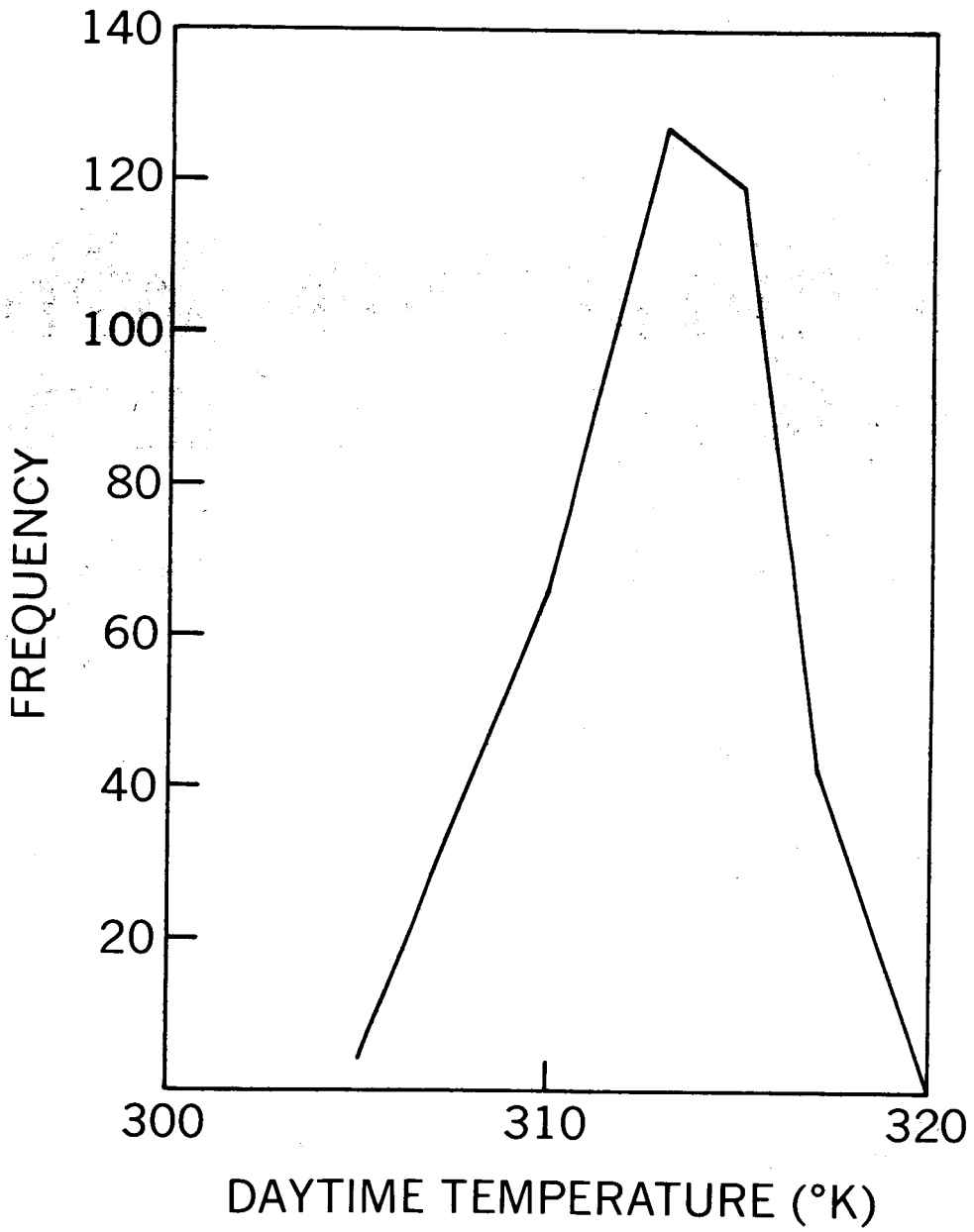

Figure 13. Frequency Distribution of Daytime Temperature, HRIR I, Sept. 2, 1964, Orbit 80, 38° S, 116.5° W

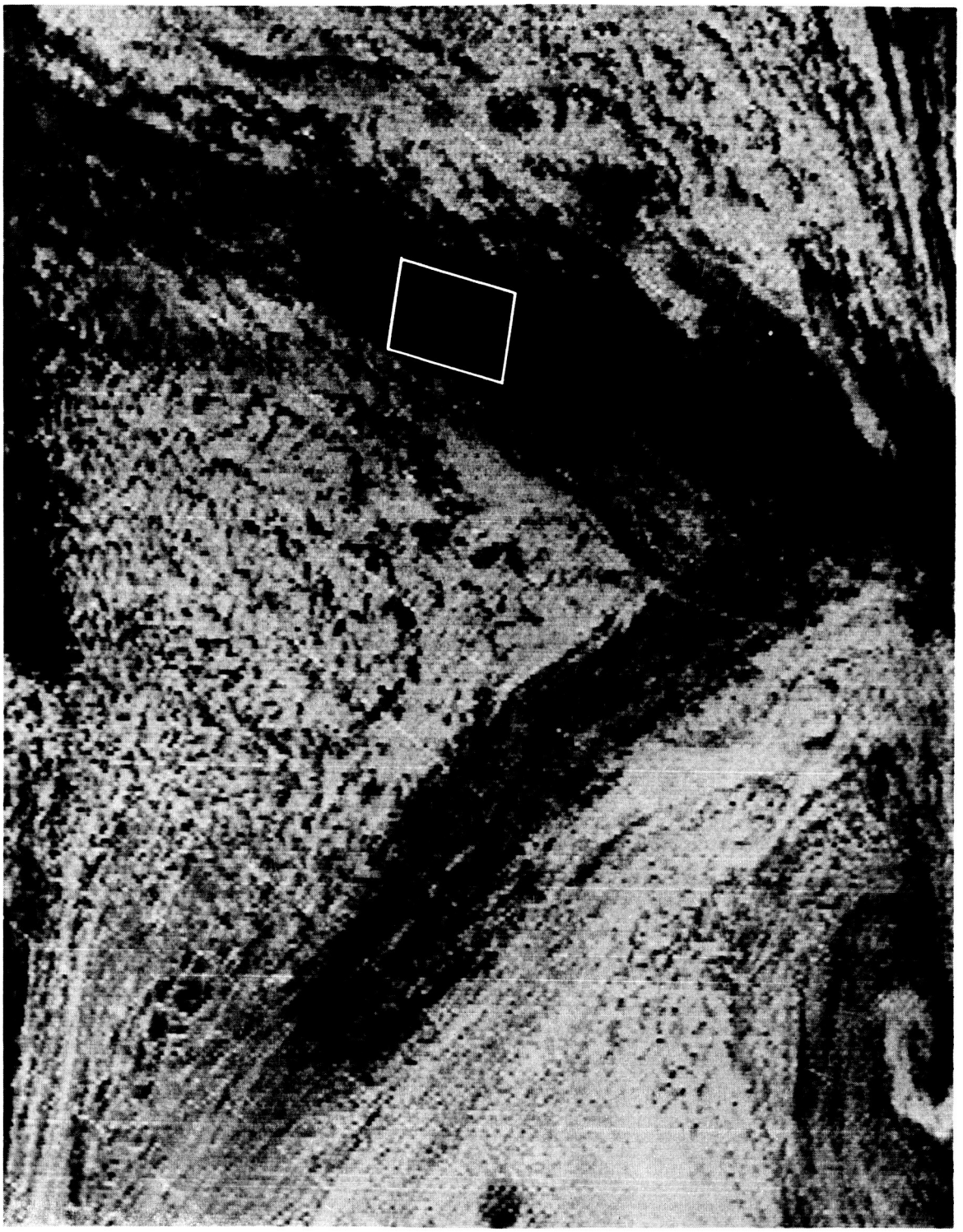

Figure 12. Infrared Photofacsimile, HRIR I, Sept. 2, 1964, Orbit 80, 38° S, 116.5° W

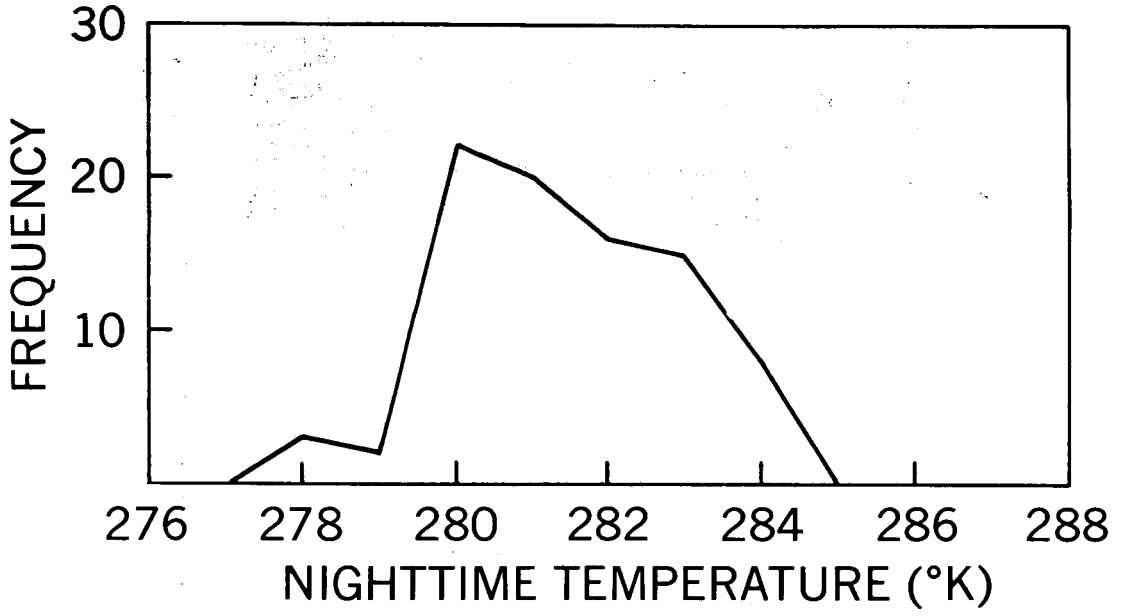

Figure 15. Frequency Distribution of Nighttime Temperature, HRIR I, Sept. 2, 1964, Orbit 73, 47° S, 139° W

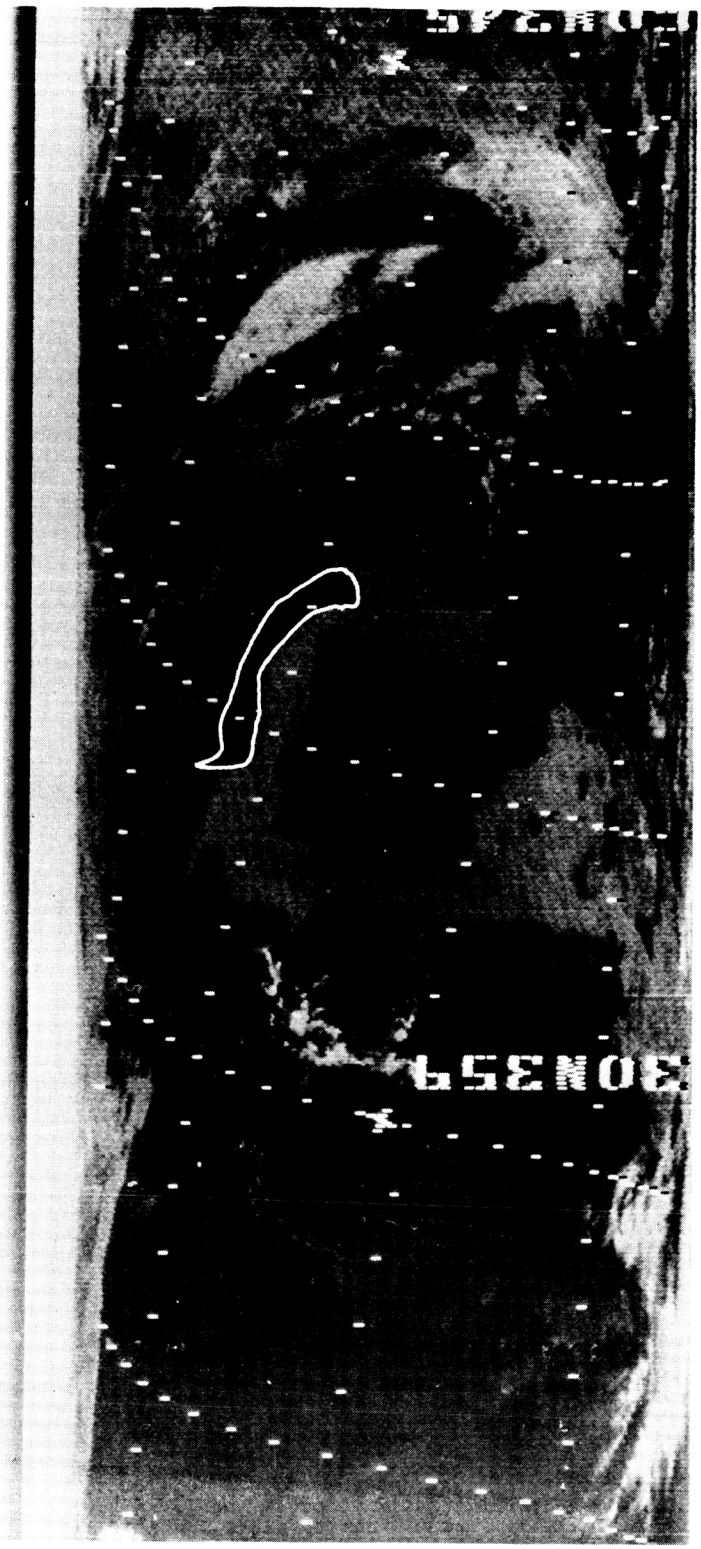

Figure 16. Infrared Photofacsimile, HRIR II, May 21, 1966, Orbit 82, 42° N, 10° W

Figure 17. Visible Picture, HRIR II, May 21, 1966, Orbit 82, 42° N, 10° W

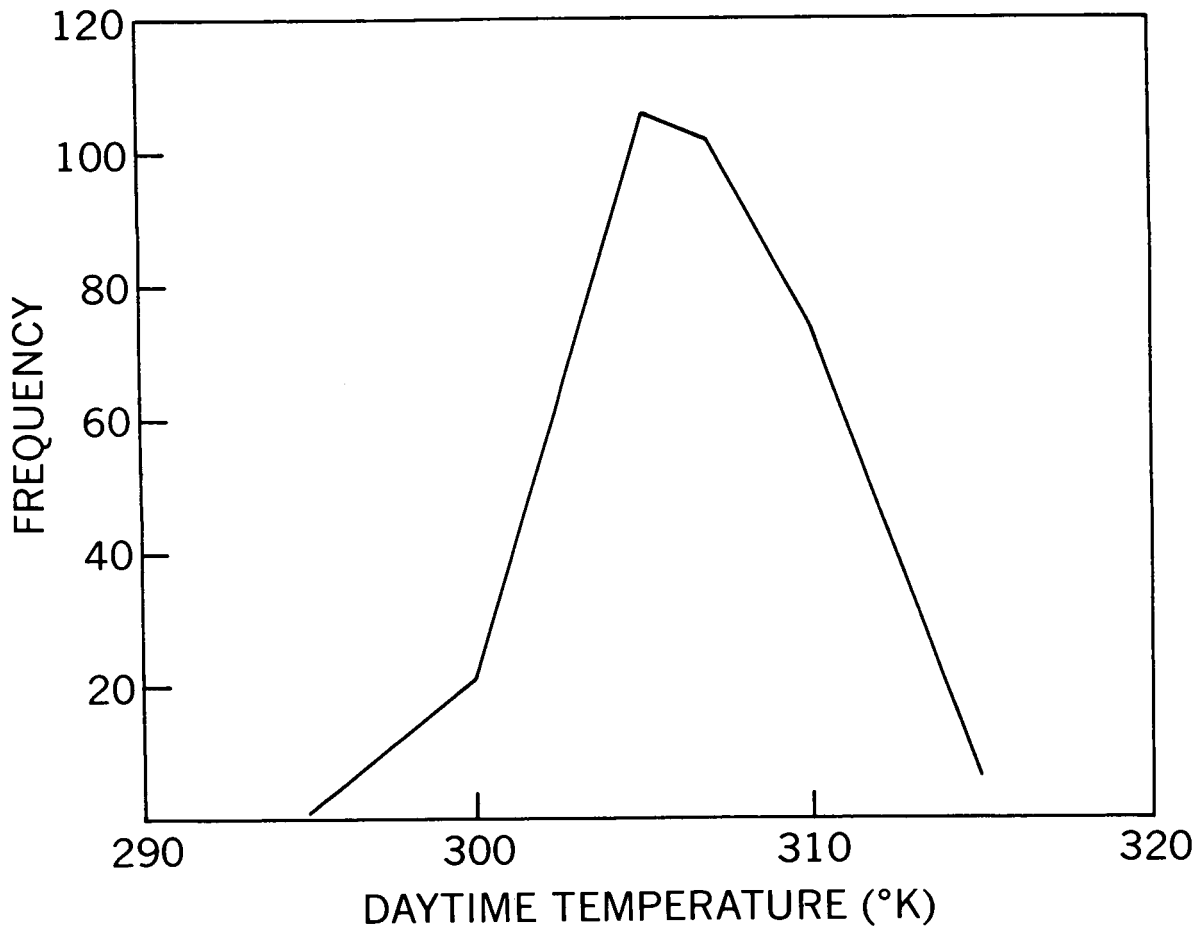

Figure 18. Frequency Distribution of Daytime Temperature, HRIR II, May 21, 1966, Orbit 82, 42° N, 10° W

Figure 19. Infrared Photofacsimile, HRIR II, May 22, 1966, Orbit 95, 41.5° N, 4.5° E

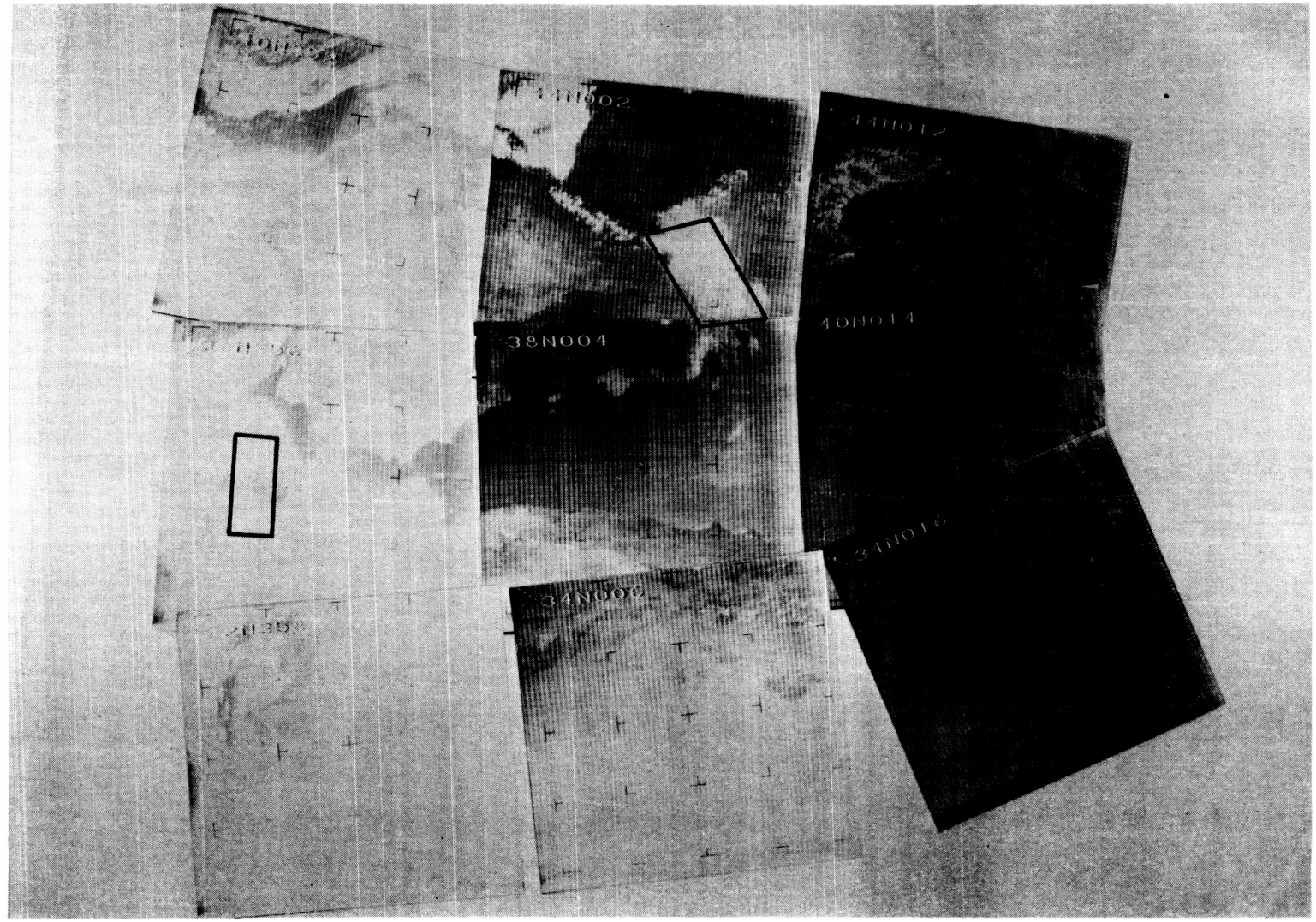

Figure 20. Visible Picture, HRIR II, May 22, 1966, Orbit 95, 41.5° N, 4.5° E

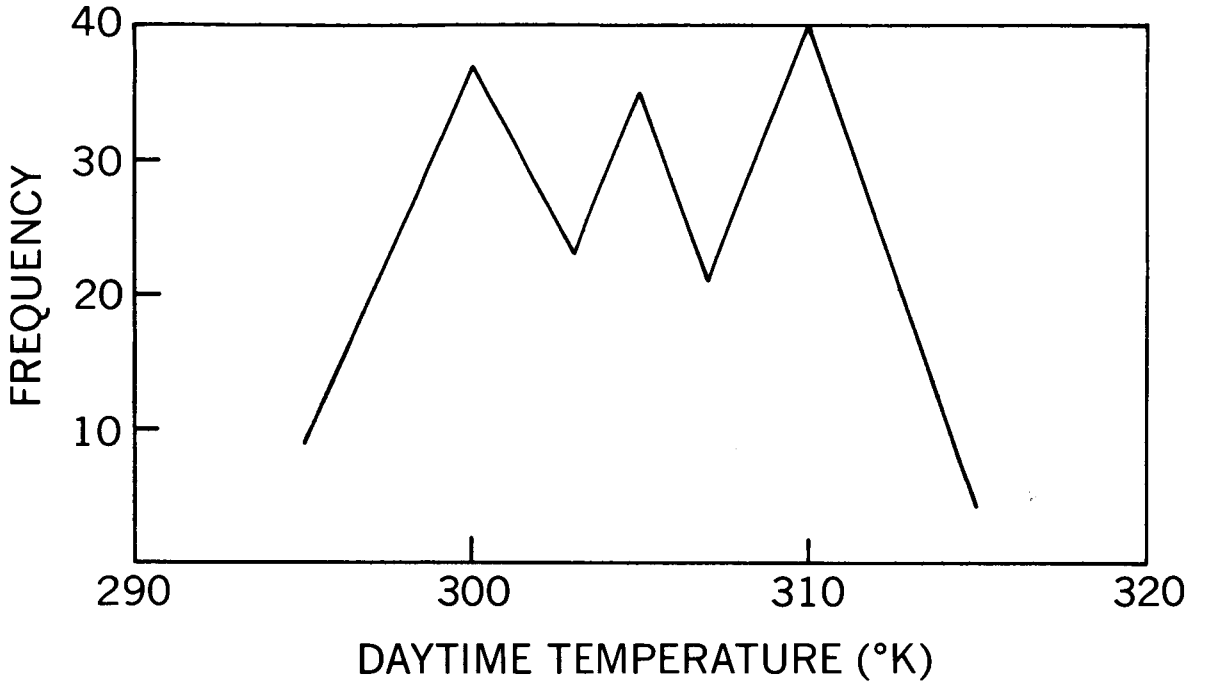

Figure 21. Frequency Distribution of Daytime Temperature, HRIR II, May 22, 1966, Orbit 95, 41.5° N, 4.5° E

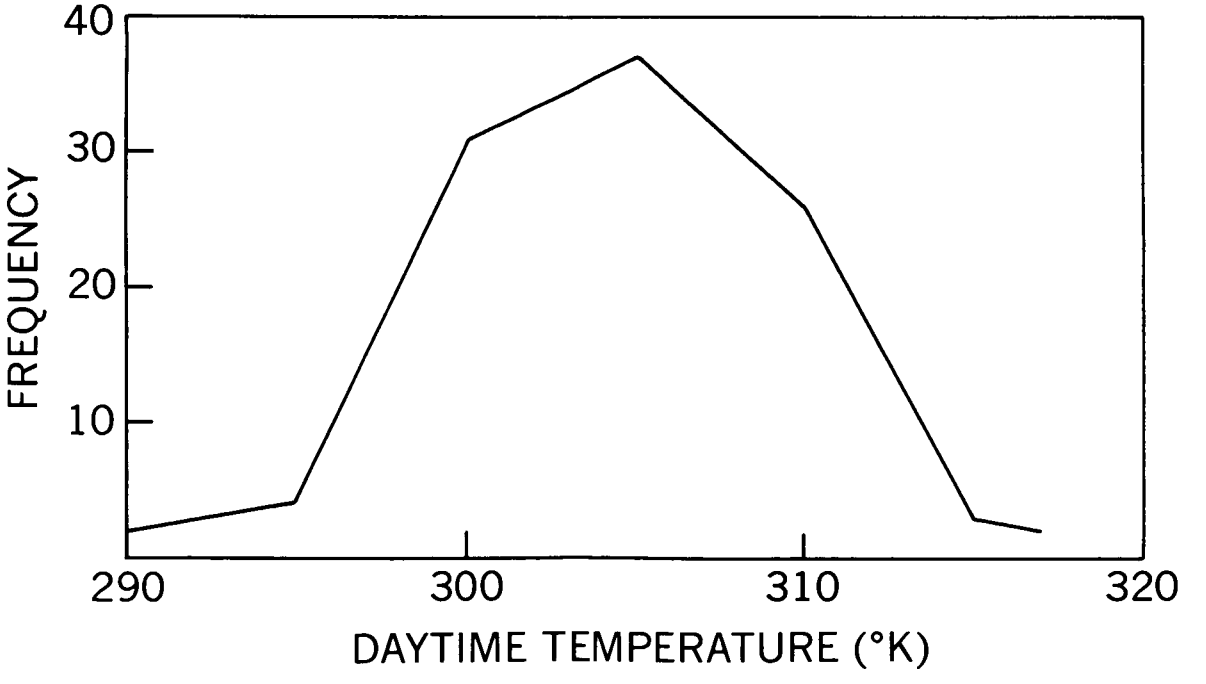

Figure 22. Frequency Distribution of Daytime Temperature, HRIR II, May 22, 1966, Orbit 95, 34-5° N, 10.5° W

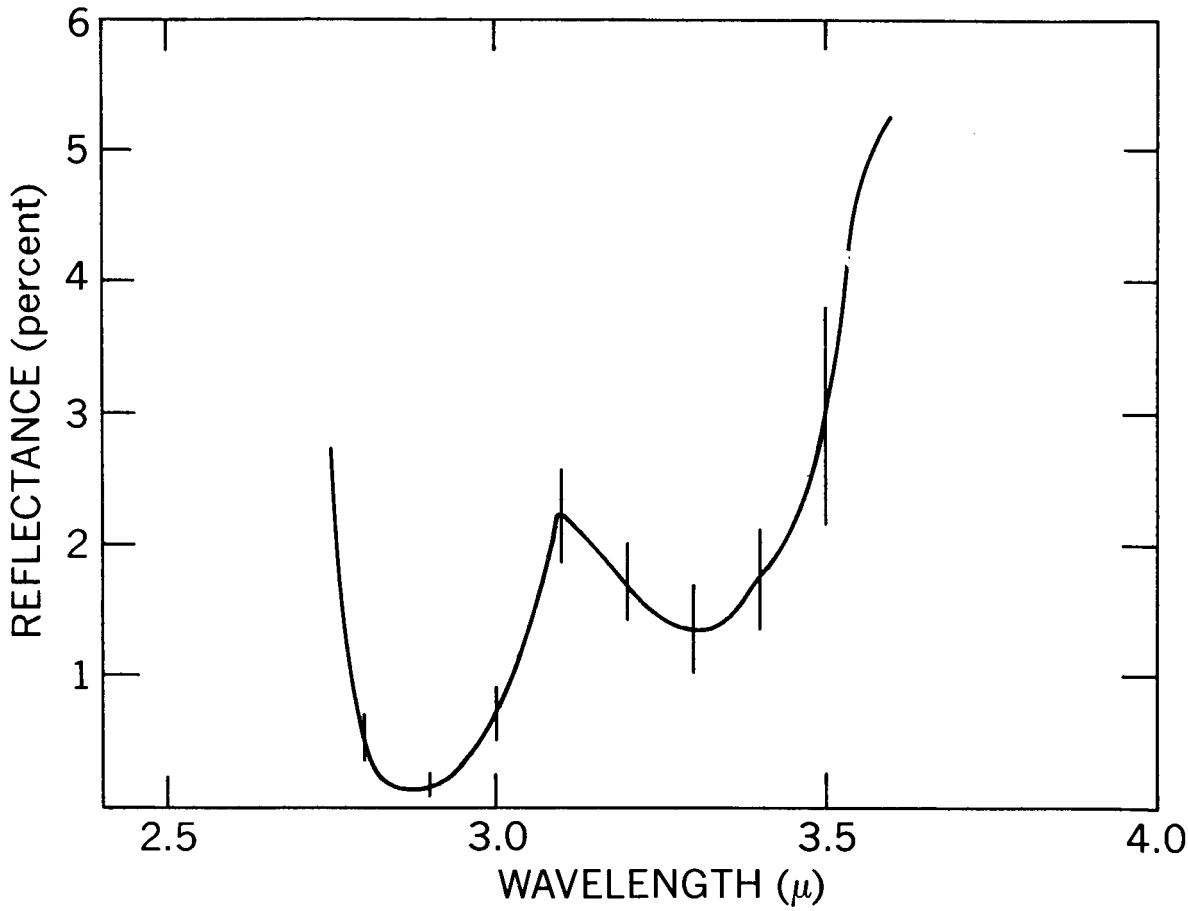

Figure 23. Spectral Cloud Reflectance after (5)

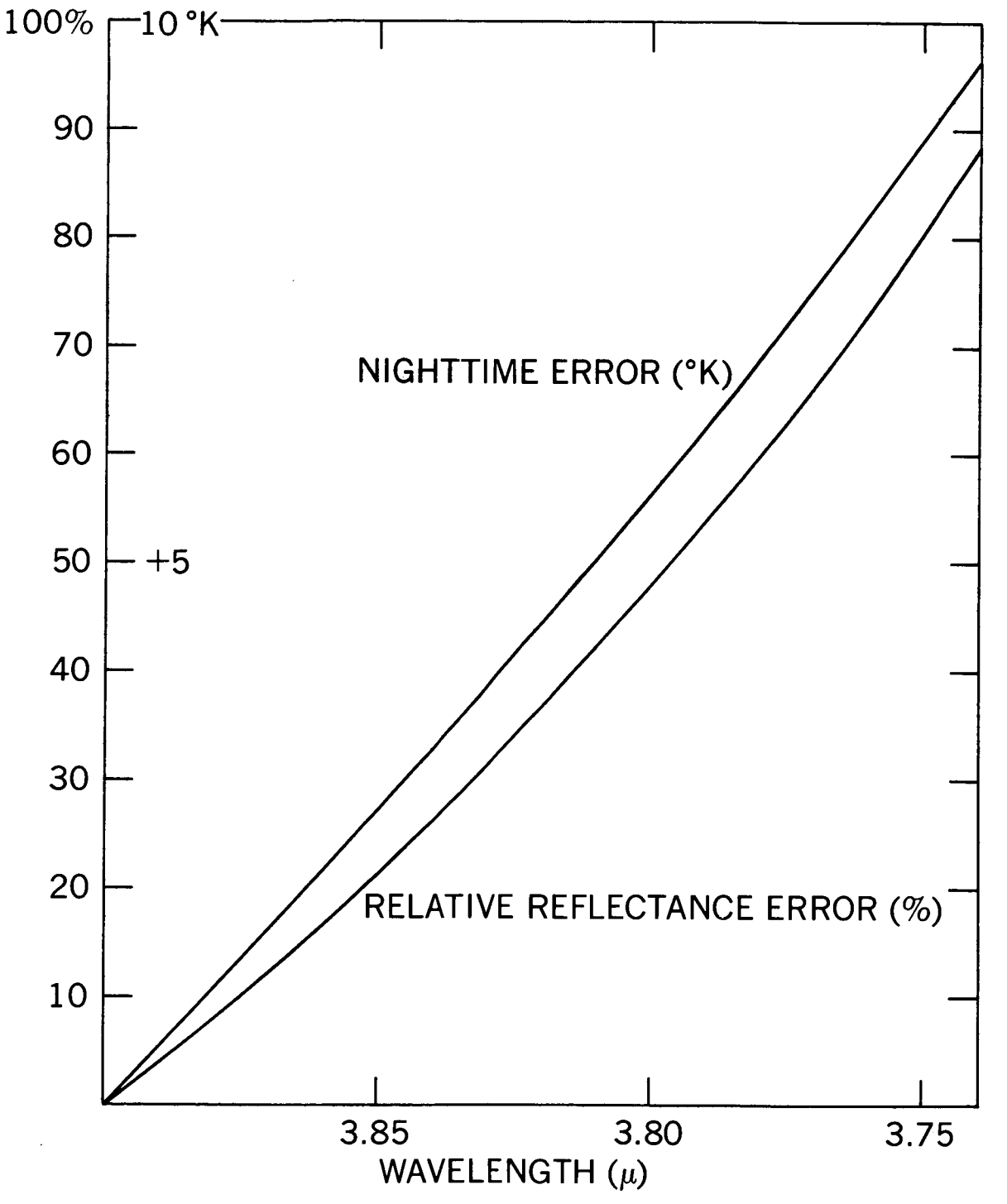

Figure 24. Daytime and Nighttime Error versus Peak Transmission Wavelength